Scientific Reports

https://doi.org/10.1038/s41598-026-39817-5

Article in Press

DEM study of fines content effects on shear strength of binary mixtures under low confining pressure

Received: 15 December 2025

Accepted: 9 February 2026

Published online: 11 February 2026

Cite this article as: Tiantian H., Zhicheng G., Chaojie Z. *et al.* DEM study of fines content effects on shear strength of binary mixtures under low confining pressure. *Sci Rep* (2026). https://doi.org/10.1038/s41598-026-39817-5

Hu Tiantian, Gao Zhicheng, Zhang Chaojie & Wang Jing

DEM study of fines content effects on shear strength of binary mixtures under low confining pressure

Hu Tiantian[1,2], Gao Zhicheng[3], Zhang Chaojie[1,2], Wang Jing[4*]

[1] Zhejiang Institute of Hydraulics & Estuary (Zhejiang Institute of Marine Planning and Design), Hangzhou, China, 310020.

[2] Zhejiang Key Laboratory of River-Lake Water Network Health Restoration, Hangzhou, China, 310020.

[3] Center for Hypergravity Experimental and Interdisciplinary Research, Zhejiang University, Hangzhou, China, 310058.

[4] Institute of Geotechnical Engineering, Zhejiang University, Hangzhou, China, 310058.

[*]Corresponding author is Wang Jing (j.wang@zju.edu.cn)

Abstract: The presence of fines in granular materials significantly affects their shear strength, particularly under low confining pressure conditions. In this study, drained triaxial compression tests were simulated using the discrete element method on spherical granular assemblies with varying fines content f_c and confining pressures σ_c to investigate the influence of f_c on the macroscopic mechanical response and underlying micro-mechanical mechanisms. Macroscopic results show that the global void ratio exhibits a non-monotonic trend, first increasing and then decreasing whereas the skeletal void ratio monotonically decreases with increasing f_c. The peak stress ratio η_p rapidly increases initially and then stabilizes above a certain critical confining pressure p_1. Intriguingly, this p_1 is found to approximately decrease as the f_c increases. At high fines content, many fine particles initially act as rattlers under low confining pressure but progressively become incorporated into load-bearing force chains as the confining pressure increases. This

mobilization enhances coarse–fine contacts, thereby contributing additional shear strength to the assembly. Based on these findings, an improved failure criterion is proposed, which accurately predicts the shear strength of granular materials across different fines contents and effectively captures its nonlinear variation under low confining pressures.

Keywords: Binary Mixtures; Low Confining Pressure; Fines Content; Shear Strength; Discrete Element Method.

1 Introduction

Shear strength parameters are among the most critical factors in geotechnical engineering design, directly governing the stability of slopes, the bearing capacity of foundations, and the safety of embankment projects. In recent years, the mechanical behavior of soils under low confining pressure conditions has attracted increasing attention. This focus is driven not only by its critical relevance to engineering constructions such as high-speed rail subgrades[1], submarine pipeline installation[2], delta reclamation [3], and lunar exploration [4], but also by its role as the theoretical foundation for mitigating geological hazards like earthquake-induced liquefaction [5] and shallow landslides [6].However, experimental investigations into the low-confining-pressure regime face numerous challenges, primarily due to difficulties in precisely controlling the stress conditions, interference from mechanical friction within testing apparatus, and the demanding requirements

for accurate stress measurement[7-10]. Consequently, the traditional approach often involves extrapolating strength parameters, which are obtained from tests conducted at 50 kPa or higher confining pressures, down to the low-stress range using conventional failure criteria. While this simplification offers practical utility in engineering applications, it overlooks the fact that the strength indices (such as peak friction angle or peak stress ratio) of granular materials are nonlinearly influenced by confining pressure in the low-stress range. This omission often leads to significant deviations between predicted and actual strength values.

This study compiles a selection of recent research findings concerning the mechanical behavior of granular materials under low confining pressure, as summarized in Table 1. The strength characteristics of granular materials are collectively influenced by a multitude of factors, including particle morphology, particle size distribution, and testing conditions [11, 12]. This dependence becomes even more pronounced, resulting in highly complex nonlinear behavior specifically in the low-stress regime. Consequently, significant discrepancies, and even contradictory conclusions, have been reported by various researchers employing different materials and testing methodologies to investigate low-confining-pressure

behavior [8]. Therefore, a more comprehensive and accurate understanding of the strength characteristics of granular materials under low confining pressure necessitates an in-depth exploration of the material's intrinsic properties, the process of structural evolution, and the underlying microscopic mechanisms.

Table 1 Summary of the shear strength variation under low confining pressure

Reference	σ_c (kPa)	Testing materials	The variation of peak stress ratio with increasing confining pressure
Ponce et al. [13]	1.38~200	Quartz sand	Decrease first and then stabilize when $\sigma_c \geq 20$ kPa
Indraratna et al. [14]	15~240	Ballast	Decrease according to a power law
Alshibli et al. [4, 15]	10~200	Lunar simulatant (Experiment & DEM)	Quickly decrease.
Fukushima et al. [8]	2~392	Toyoura sand	Within 50 kPa, there is a slight increase but little change, while above 50 kPa, there is a significant decrease
White [7]	6~400	Leighton Buzzard sand	Tensile stress ratio increases significantly within 25kPa and then turns to decrease. Compressive stress ratio initially increases slightly and then decreases.
Nguyen et al. [16]	0.3-1000	Ellipsoid with rolling resistance model (DEM)	First increase and then decrease, with a turning point of 50kPa
Xiao et al. [17]	50~400	Spherical and crushed glass beads	The spherical glass beads rapidly increase and then stable; the crushed glass beads decrease approximately linearly.
Vinod et al. [18, 19]	25~180	Sphere with Hertz model (DEM)	Increase from 1.3 to 1.5
Jiang et al. [20]	100~3000	Rod-shaped particles	Decrease from 1.7 to 1.5

Furthermore, natural soils typically contain a certain proportion of fine particles resulting from weathering, crushing, and transport

processes. In geohazards such as soil liquefaction, seepage-induced piping, and subgrade settlement, the presence and migration of fines are recognized as critical factors triggering failure [21, 22]. As the fines content f_c increases, the primary mechanical skeleton, initially composed of coarse grains, is progressively transformed into a mixed fabric consisting of both coarse and fine particles. This transition significantly alters the pore structure, particle contact states, and overall shear strength characteristics [23, 24]. Existing literature indicates that the influence of fines on shear strength is far from uniform. Some studies suggest that fines fill the interstitial voids, thereby enhancing the shear strength under drained conditions[25-27]. Conversely, other researchers have pointed out that non-plastic fines have a negligible effect [21] or may even exert a weakening effect [28, 29]. For instance, Yang et al. [30] demonstrated that particle shape also plays a decisive role: the addition of crushed quartz slightly increased the critical state friction angle, whereas the inclusion of spherical glass beads led to a marked reduction in strength. Chung et al.[31] and Liao et al.[32] found through rotating drum experiments that increasing fine content enhances lubrication effect and energy input, thereby promoting size-induced granular segregation. Overall, while previous research has extensively investigated the effects of

fines under specific stress states, few studies have addressed the evolution of contact states and the complex interaction between coarse and fine particles across varying stress regimes, particularly in the low-confining-pressure range.

Given the inherent limitations of experimental testing at low confining pressures and the intricate interaction mechanisms between coarse and fine particles, the Discrete Element Method (DEM) has increasingly been adopted to simulate the behavior of granular materials at the micro-scale. Gong et al. [33] utilized DEM to verify the effects of fines content and particle shape on both peak and critical state friction angles. By categorizing contacts into three types, they demonstrated that more complex fines shapes contribute more significantly to shear strength through coarse-fine and coarse-coarse contacts, while the contribution of fine-fine contacts remains negligible. Furthermore, studies by Hu et al. [34] and Dai et al. [35] under drained and undrained conditions, respectively, revealed that the primary force-chain skeleton formed by coarse particles is prone to instability without the lateral support of fines, potentially leading to liquefaction or strength degradation. DEM not only allows for the precise application of low confining stresses via servo-control mechanisms but also enables the tracking of micro-mechanical

responses, such as the evolution of force chains and changes in coordination numbers. This makes it an ideal tool for investigating the mechanical properties of coarse-fine mixtures in the low-stress regime.

Against this background, this study employs DEM simulations to construct a series of specimen assemblies with varying fines contents. Drained triaxial compression tests are simulated across a range of confining pressures, with a specific focus on the low-confining-pressure regime. The objectives are to characterize the influence of fines content on the macroscopic strength of binary mixtures and to elucidate the underlying micro-mechanical mechanisms. Finally, a shear strength failure criterion that explicitly accounts for the effect of fines content is proposed to provide scientific guidance for geotechnical engineering design under low-stress conditions.

2 Numerical Procedures

2.1 Discrete Element Method Simulation Procedure

The numerical simulation software used in this study is PFC3D, a discrete element software developed by Itasca [36]. The numerical simulation procedure for the drained triaxial compression tests precisely follows the steps of a standard laboratory test: specimen preparation, consolidation, and shear loading. Figure 1 illustrates

the geometry of the DEM specimen and the procedure of the triaxial test. During specimen preparation, a large number of coarse and fine particles are generated within the boundaries of a cubical cell enclosed by six smooth rigid walls. A very small initial isotropic confining pressure, e.g., 10 kPa, is applied to the specimen using a servo-control technique, by moving the wall boundaries towards the center to achieve particle cluster aggregation. For quasi-static loading conditions, the axial stress σ_a and the lateral confining pressure σ_c are determined based on the ratio of the normal contact force f_n on the boundary walls to the wall area A_w:

$$s_i = \frac{1}{A_w} \sum_{j \in A_w} f_{n,j} \tag{1}$$

After the specimen reaches a quasi-static equilibrium state under the initial 10 kPa confining pressure (typically assessed by an unbalanced force ratio less than 0.01%), the servo-control is continuously utilized to gradually increase the confining pressure, consolidating the specimen to the target confining pressure value. In the shear loading stage, the top and bottom walls are displaced towards each other at a constant, sufficiently slow velocity to achieve axial compression, thereby ensuring quasi-static loading. Concurrently, the lateral walls continuously adjust their positions via servo-control to maintain a constant confining pressure, simulating

the drained condition. The shear loading is terminated when the axial strain reaches 20%. The shear strength of the specimen is represented by the stress ratio, calculated as

$$h = \frac{3(s_a - s_c)}{s_a + 2s_c} \tag{2}$$

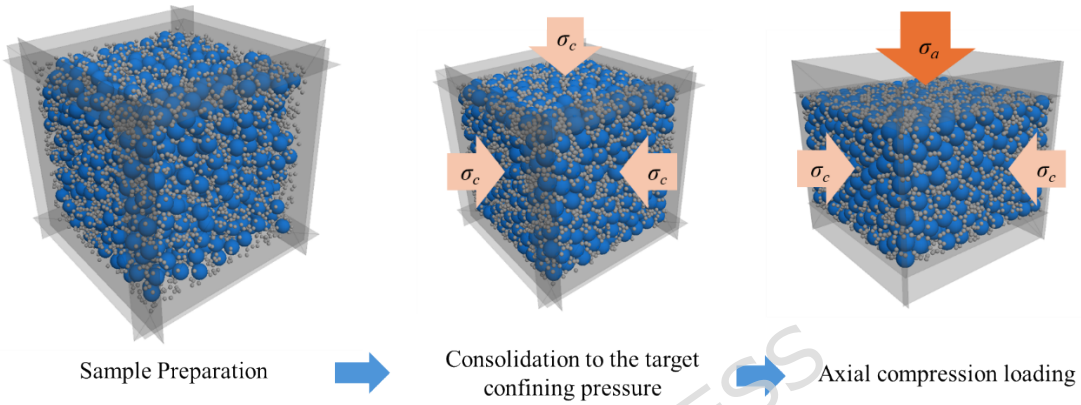

Figure 1 Schematic diagram of the triaxial test procedure

2.2 Contact Model and Parameter Calibration

The linear model was employed to govern inter-particle interactions in this study, based on several critical considerations. First, as demonstrated by Zhao et al. [37], the linear model can effectively resemble the Hertz-Mindlin model in terms of both macroscopic responses (such as shear strength and volumetric strain) and microscopic characteristics (such as the probability distribution function of contact forces) under quasi-static loading conditions. Specifically regarding large size ratios, Liu et al. [38] simulated the behavior of gap-graded soils with large particle size ratios using the linear model and found their research conclusions consistent with prior DEM studies using the Hertz–Mindlin contact

model [39]. Furthermore, to ensure quasi-static conditions under low confining pressures, a very low axial loading rate was adopted in this study. This necessitated substantial computational time. The linear model was selected over the Hertz–Mindlin model for its significantly higher computational efficiency[38, 40].

In the linear contact model, the normal contact force f_n is linearly proportional to the normal overlap x_n, with the proportionality constant being the normal stiffness k_n. The tangential force f_s is computed based on the tangential force from the previous time step f_{s0}, the tangential displacement increment Δx_s, and the tangential stiffness k_s:

$$\begin{aligned} f_n &= k_n x_n \\ f_s &= f_{s0} + k_s \Delta x_s \end{aligned} \tag{3}$$

The accurate selection of contact model parameters is essential for ensuring the reliability and validity of the simulation results. Therefore, prior to investigating the effect of fines content, a comprehensive parameter calibration procedure was performed against the drained triaxial test results on glass bead specimens reported by Wu et al. [41].

The specimens used by Wu et al. consisted of 4700 glass beads with a diameter of 4 mm and a density of 2530 kg/m^3, exhibiting an initial void ratio of approximately 0.55. Drained triaxial tests were

conducted after consolidating the specimens at 100 kPa, 200 kPa, 300 kPa confining pressures, up to a maximum axial strain of 15%. Figure 2 presents the experimental variation of deviator stress with axial strain under these different confining pressures. In this study, DEM specimens were generated to match the key geometric features (particle size, density, and void ratio) of the physical tests. A preliminary range for the contact parameters was established based on existing literature[42-44]. Subsequently, a systematic trial-and-error approach was conducted within this range to achieve close agreement between the simulated shear strength and the experimental results. As illustrated in Figure 2, the simulation accurately captures the evolution of deviator stress with axial strain under varying confining pressures. The final calibrated contact model parameters are listed in Table 2. More detailed procedures for the calibration can be referenced in the work by Ling et al. [45].

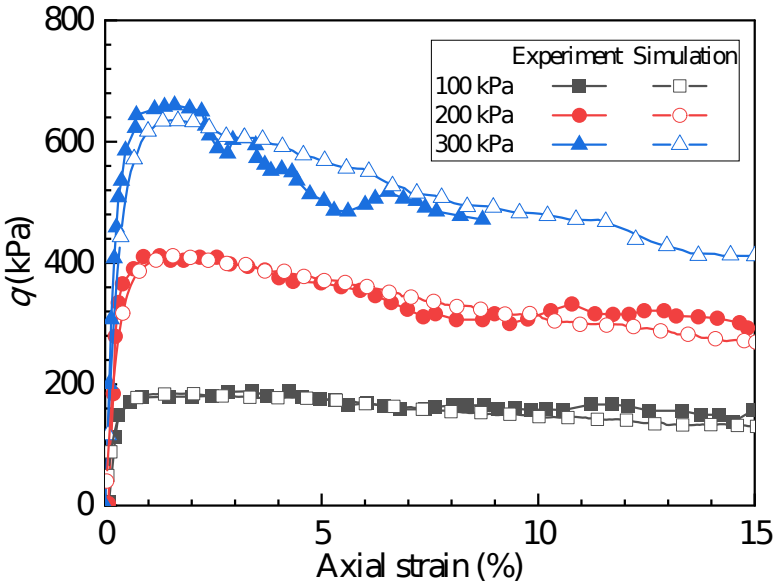

Figure 2 Comparison of triaxial test and DEM simulation results

Table 2 Parameters of the Contact Model

Parameter name	Parameter value
Wall normal stiffness (N/m)	10^7
Particle normal stiffness (n/m)	400 MPa×r
Stiffness ratio	1
Inter-particle friction coefficient	0.5
Particle density (kg/m^3)	2530
Damping coefficient	0.7

The stress state of the specimen can be determined either by the contact forces acting on the boundaries (Eq. (1)) or by the stress tensor derived from contact forces [46]. As illustrated in Figure 3, these two methods yield nearly identical results under conditions of smooth wall boundaries and quasi-static loading. The consistency between these two approaches has also been verified in the study by Li et al. [47, 48].

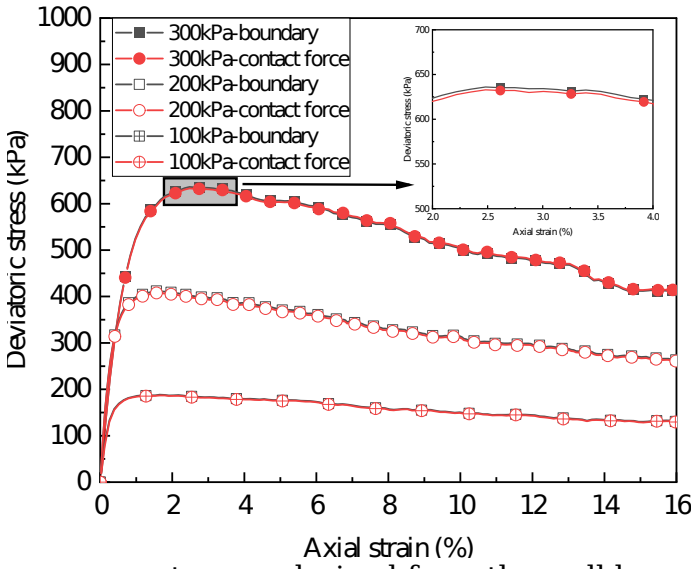

Figure 3 Stress curves stresses derived from the wall boundaries and the contact force

2.3 Testing Conditions

Based on previous studies [33], the mass fraction of fines content in natural soils is typically less than 20%, a range where the granular skeleton is considered to be in an under-filled state. Therefore, this study primarily investigates specimens with fines contents below 30%. A series of specimens were set up with fines contents of 0%, 5%, 10%, 15%, 20%, 25%, and 30%. Table 3 summarizes the number of coarse particles, fine particles, total particles, and the initial void ratio at a confining pressure of 10 kPa for each specimen group. The mean diameter of the coarse particles is 0.216 mm, which is similar to the average particle size of Toyoura sand [49]. The ratio of coarse to fine particle diameters is set to 4, which is consistent with values adopted in previous literature [50, 51] (where the particle size ratios were 3.9 and 4.5, respectively)

Table 3 Number of particles in specimens with different fines

contents

Fines content	Total number of particles	Number of coarse particles	Number of fine particles	Initial void ratio
0%	14169	14169	0	0.639
5%	16474	3775	12699	0.573
10%	32081	3959	28122	0.496
15%	41489	3378	38111	0.431
20%	31247	1839	29408	0.392
25%	32726	1466	31260	0.366
30%	33332	1173	32159	0.375

To ensure that specimens with different fines contents possess comparable relative densities, the particle friction coefficient was initially set to zero during the specimen generation process to achieve the densest state. The friction coefficient was then restored to 0.5 for the subsequent consolidation and shear stages. Furthermore, before initiating the drained shearing phase, the specimens were consolidated to the target confining pressure. To compare the mechanical characteristics of the granular assemblies under both high and low confining pressures, the range of consolidation pressures considered in this study spans from 10 to 1000 kPa. Accordingly, a total of 70 drained triaxial compression test

simulations were performed, comprising 7 different fines contents and 10 distinct confining pressures. To maintain quasi-static loading conditions, especially for the low confining pressure tests where contact forces are smaller, the axial loading rate needed to be further reduced. The specific axial loading rates for different confining pressures and corresponding inertial numbers are summarized in Table 4. The inertial number is calculated according to the following equation:

$$I = \frac{\dot{\epsilon}_a d}{\sqrt{p/\rho}} \quad (4)$$

Where $\dot{\epsilon}_a$ is the axial strain rate, d is the average particle diameter, approximated by the mean size of coarse and fine particles, p is the mean stress, approximated by the confining pressure, and ρ is the particle density. It is evident that the loading rates used in this study meet the quasi-static condition in terms of the inertial number (I<1×10^{-3}[52]; I<7.9×10^{-5}[53]).

Table 4 Axial loading rate under different confining pressures.

Confining pressure (kPa)	10	20	50	100~1000
Axial strain rate (s^{-1})	0.08	0.25	0.5	1
Inertial	0.56×10^{-}	1.23×10^{-}	1.55×10^{-}	0.69×10^{-}

number	5	5	5	$5\sim2.20\times10^{-5}$

3 Results and Discussion

3.1 Consolidation Tests

Figure 4 displays the DEM samples prepared with varying fines contents, demonstrating a uniform distribution of coarse and fine particles. The isotropic consolidation curves corresponding to these specimens are plotted in Figure 5(a). At a low fines content (e.g., f_c =10%), the force-transmitting skeleton is predominantly constituted by coarse grains, with fine particles filling the voids between the coarse particles. However, with a further increase in fines content (e.g., f_c=30%), the microstructure undergoes a transition from a skeleton dominated by coarse grains to a composite fabric in which coarse and fine particles jointly bear the effective stress.

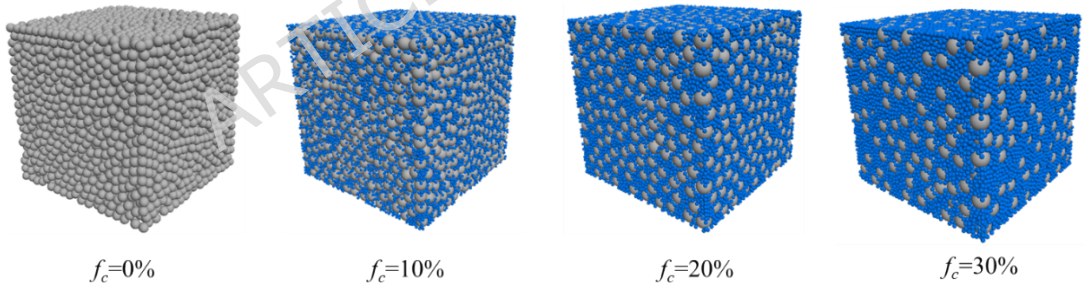

Figure 4 Specimens with varying fines contents

Figure 5 illustrates the isotropic consolidation curves of specimens with varying fines contents. With increasing consolidation pressure, the void ratio exhibits consistent decreasing trends. As the fines content increases, fine particles occupy more inter-coarse voids, leading to a denser packing structure. Consequently, the

consolidation curves shift downwards within the □-□ plane.

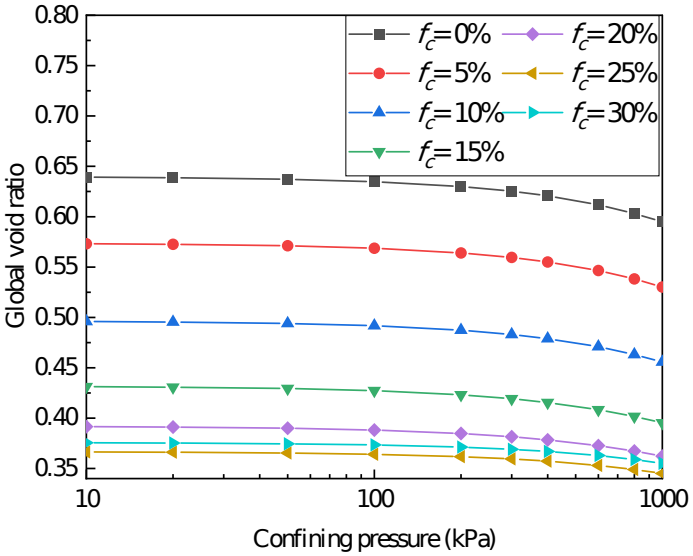

Figure 5 Consolidation curves of specimens with varying fines contents

In binary mixtures, particularly in the underfilled state with a low fines content, a portion of the fine particles exist as "rattlers" [34]. Rattlers characterized by a coordination number of less than 4, are mechanically unstable; although they occupy the void space, they do not participate in the transmission of external loads. Consequently, several researchers have adopted the concept of skeleton void ratio to characterize the actual load-bearing structure of the specimen [50, 54, 55]. In the calculation of the skeleton void ratio, rattlers are treated as part of the void space:

$$e^* = \frac{V_v + V_r}{V_p - V_r} \tag{5}$$

Where V_v, V_r, and V_p represent the volume of voids, the volume of rattlers, and the total volume of particles in the specimen, respectively. Following the approach in Ref. [55], the conventional

void ratio is referred to as the “global void ratio” in the following text to distinguish it from the skeleton void ratio.

In this study, we adopt the definition from Ref. [56], where rattlers are identified as those with a coordination number CN of less than 4. Some researchers [57] define rattlers as having a coordination number of less than 2. Figure 6 presents the distribution of coordination numbers for specimens with fines contents of 10%, 20%, and 30% under a confining pressure of 100 kPa. The fraction of particles with coordination numbers of 1, 2, or 3 is significantly smaller than those with a coordination number of zero. This is because a spherical particle requires at least four contacts to achieve mechanical stability[56]. Therefore, the choice between these two definitions ($CN < 4$ or $CN \leq 1$) has a negligible impact on the calculation of the skeleton void ratio.

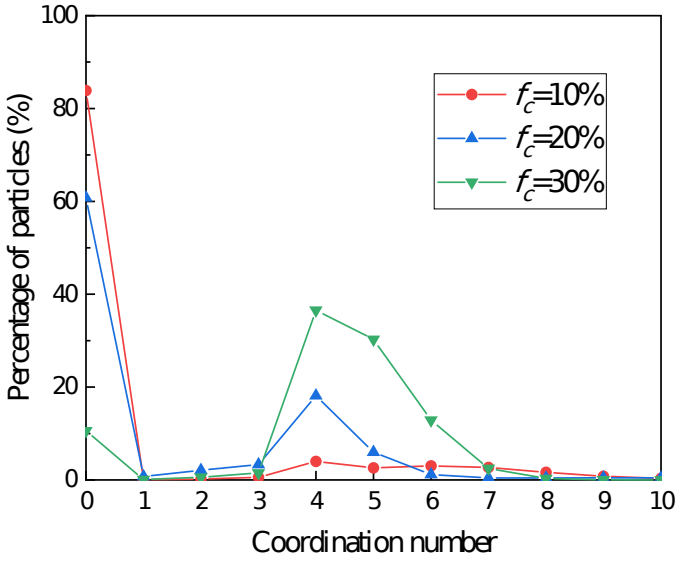

Figure 6 The distribution of coordination number

In contrast to the global void ratio shown in Figure 5, the evolution of the skeleton void ratio e^* for specimens with different fines contents exhibits significant differences, as illustrated in Figure 7. When $f_c \leq 10\%$, e^* decreases slowly with increasing confining pressure. This is because the fines content is low, and the fine particles remain as rattlers even after consolidation, having a negligible effect on the particle composition of the force-transmitting skeleton. Figure 8 presents the statistics regarding the proportion of fine particles existing as rattlers. It can be observed that for $f_c \leq 10\%$, nearly all fine particles are rattlers at a confining pressure of 10 kPa. Even when the confining pressure increases to 1000 kPa, more than 90% of the fine particles remain as rattlers.

When f_c increases to 20%, the influence of fines content on the skeleton void ratio intensifies. The coarse-grain skeleton possesses large voids ($e^*=0.64$) at a low confining pressure of 10 kPa, with 80% of fine particles existing as rattlers within the voids. However, the skeleton compresses as the confining pressure increases. The rattlers establish contacts with surrounding particles and transition into components of the force chains, leading to a rapid decrease in both the rattler proportion and the skeleton void ratio. For the specimen with $f_c = 20\%$, although the variation in global void ratio

is similar to that of other specimens (Figure 5), the sharp decline in skeleton void ratio indicates that the force-transmitting skeleton has undergone significant changes.

For the specimen with f_c=30%, the variation of e^* with confining pressure is very gentle, which appears similar to the case of $f_c \leq 10\%$; however, the underlying mechanisms differ. In the former case (f_c = 30%), fine particles have sufficiently filled the voids of the coarse skeleton even at low confining pressures, resulting in a very low content of remaining rattlers (Figure 8); thus, further increasing the confining pressure has little effect on the skeleton structure. In contrast, in the latter case ($f_c \leq 10\%$), the amount of fine particles is insufficient to fill the voids within the coarse skeleton, even under increased confining pressure.

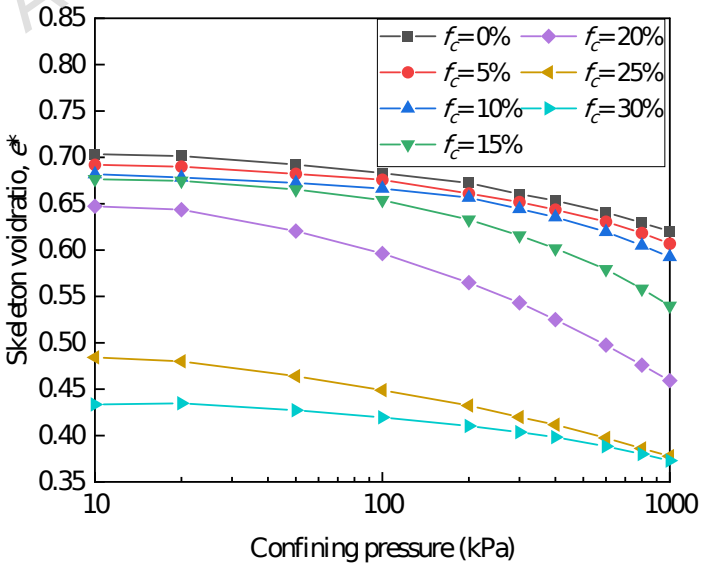

Figure 7 Skeleton void ratio of specimens with different fines contents during consolidation

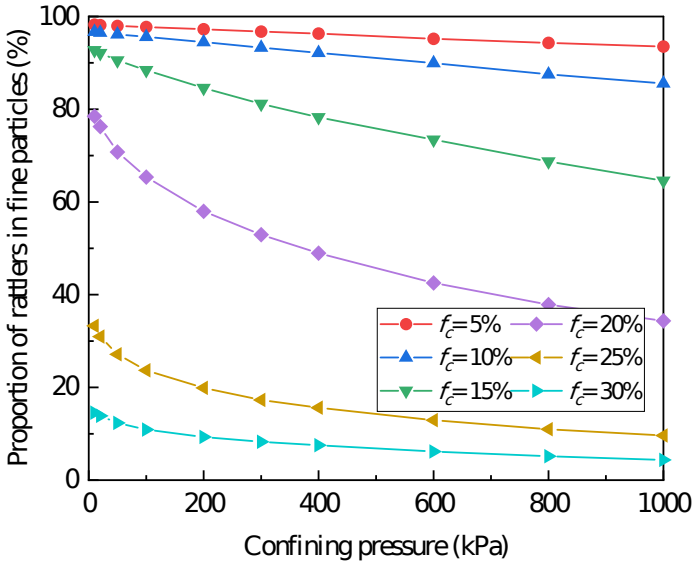

Figure 8 Proportion of fine particles existing as rattlers

Figure 9 illustrates the variations of both global void ratio and skeleton void ratio with respect to fines content under confining pressures of 10 kPa and 1000 kPa. The trends of global void ratio remain consistent across different confining pressures. As the fines content increases, the inter-granular voids between coarse grains are gradually occupied by fine particles. Consequently, the global void ratio initially decreases and then increases, reaching a minimum at f_c=25%. This indicates that the packing density of the coarse-fine mixture is maximized around f_c=25%, which aligns with previous findings [50].

Regarding the skeleton void ratio, as the fines content increases from 0% to 20%, the skeleton void ratio of the specimen at 10 kPa decreases slightly. This decline is more gradual compared to that of the global void ratio, suggesting that although the added fine

particles occupy void space, only a small fraction transform into force-chain particles. When the fines content exceeds a critical threshold of 20%, the newly added particles, together with the existing rattlers, rapidly establish contacts with surrounding particles, resulting in a precipitous drop in the skeleton void ratio.

The influence of confining pressure on the skeleton void ratio is more pronounced than on the global void ratio. First, at the same fines content, the difference in skeleton void ratio between specimens at 10 kPa and 1000 kPa is significant (approximately 0.06~0.18), whereas the difference in global void ratio is merely 0.02~0.04. According to the existing studies[39, 56], the critical fine content is a common concept in coarse-fine mixtures and its specific value is influenced by factors such as particle shape and the size ratio between coarse and fine particles. It is also found in this study that the critical fines content decreases with increasing confining pressure, as shown in Figure 9. Under high confining pressure, the voids within the coarse-grain skeleton are compressed; consequently, the rate of decrease in skeleton void ratio begins to accelerate when the fines content reaches 10%. Conversely, specimens under low confining pressure require a greater amount of fine particles to fill the void space, corresponding to a critical fines content of

approximately 20% at 10 kPa. This further indicates that soil with the same fines content exhibits distinct skeleton structures under low versus high confining pressures.

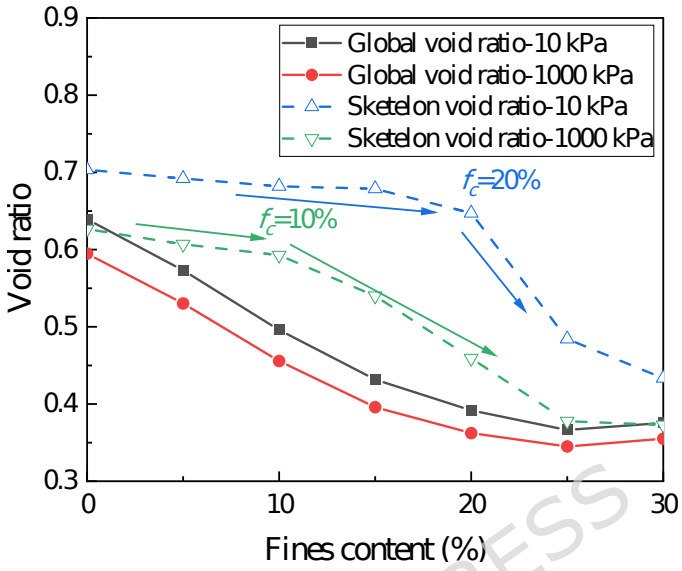

Figure 9 Variation of skeleton void ratio and global void ration with fines contents

3.2 Shear Strength

Axial compression tests were performed on the consolidated specimens to determine the evolution of the stress ratio with axial strain. The stress ratio curves for specimens with fines contents of 0%, 5%, and 20% at confining pressures of 20 kPa and 200 kPa are shown in the Figure 10. Because the specimens were prepared in a dense state, they exhibited varying degrees of strain softening, characterized by the stress ratio reaching a peak value followed by a gradual decrease. In comparison with the fines-free specimens, the specimen with f_c=5% did not show a significant increase in strength at either 20 kPa or 200 kPa. However, a notable increase in the peak

stress ratio was observed for the specimen with f_c=20%. Specifically, at a confining pressure of 20 kPa, the peak stress ratio increased from 1.0 to 1.13, while at 200 kPa, it increased from 1.1 to 1.3.

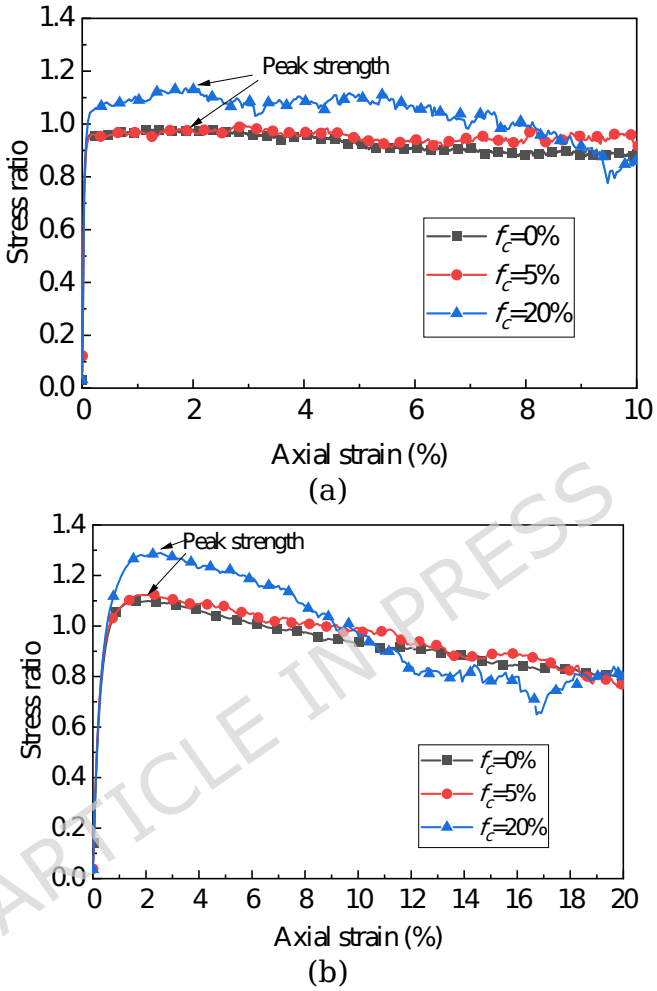

Figure 10 Stress ratio curves of specimens with varying fines contents and confining pressures: (a) σ_c=20 kPa; (b) σ_c=200 kPa.

Regarding the size effect, according to Ref. [58], size effects may occur when the specimen size ratio L/d_{max} is insufficient, leading to significant oscillations in simulated curves; specifically, a ratio of $L/d_{max} \geq 15$ has been suggested as necessary. However, other scholars [59, 60] have argued that once the specimen size ratio exceeds 8, further increases in specimen dimensions have a negligible impact

on the overall trend of the stress ratio curves. Figure 11 compares the stress ratio curves of the specimens used in this study with a larger specimen ($□/□_{max}$=15) under a confining pressure of σ_c = 200 kPa. Following the increase in specimen size, the oscillation phenomenon in the curves was indeed attenuated; however, the evolution of the stress ratio curve—particularly the peak points—remains fundamentally consistent with the results shown in Figure 10(b). Given that this study primarily focuses on shear strength, the current specimen dimensions and particle numbers are considered to satisfy the requirements for accuracy.

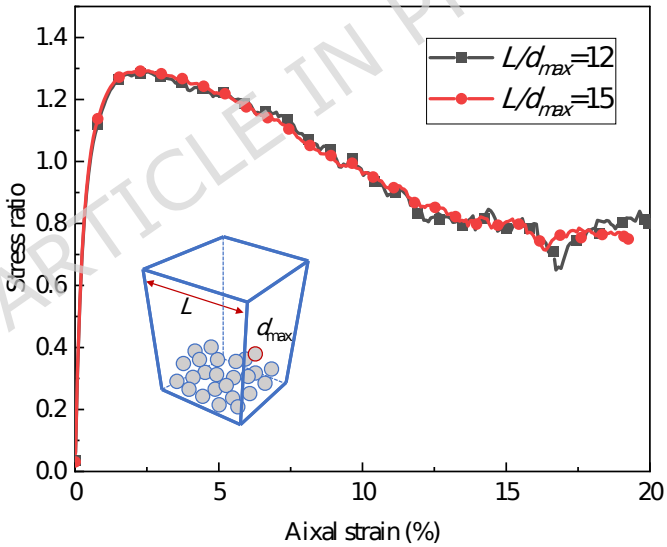

Figure 11 Stress ratio curves with different specimen sizes.

Figure 12 presents the variation of the peak stress ratio as a function of confining pressure for specimens with different fines contents. As the confining pressure increases, the peak stress ratio initially rises and subsequently stabilizes upon reaching a critical confining pressure. The influence of fines content is manifested in

two primary aspects. First, the peak stress ratio increases with fines content, which is consistent with the research findings of Zuo et al. [50]. Second, as the fines content increases, the peak stress ratio reaches its plateau at lower confining pressures, indicating a reduction in the critical confining pressure. For instance, the specimen with f_c=0% maintains an increasing trend even at 1000 kPa, whereas the specimen with f_c= 25% achieves its maximum peak stress ratio of approximately 1.44 at a confining pressure of only 200 kPa. It can be observed that the impact of fines content is significantly more pronounced under low confining pressures compared to the high-confining-pressure regime, where the peak stress ratios remain relatively stable. Specifically, a higher fines content leads to a more rapid growth of the peak stress ratio with confining pressure in the low-stress range.

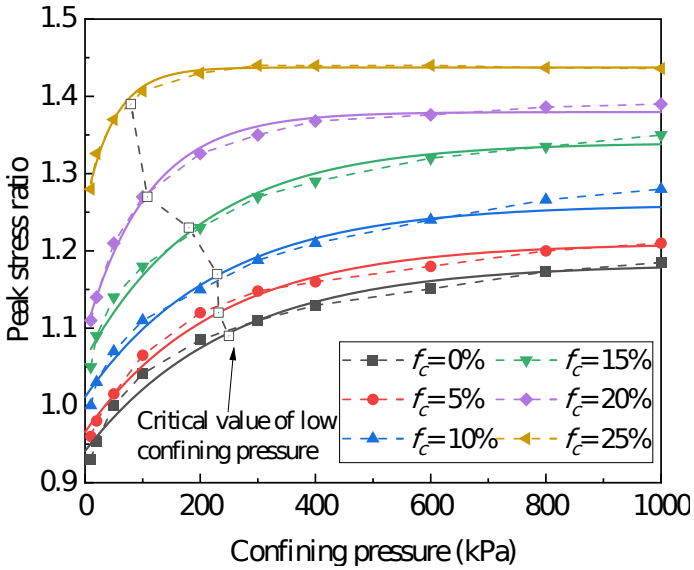

Figure 12 Variation of peak stress ratio with confining pressure for specimens with different fines contents.

To elucidate the mechanism by which fines content influences shear strength under low confining pressure, this study adopted the method proposed by Gong et al. [33] to investigate the contribution of coarse and fine particles to the overall shear strength. All contacts were categorized into three types: coarse-coarse contacts (C-C), coarse-fine contacts (C-F), and fine-fine contacts (F-F), as illustrated in Figure 13.

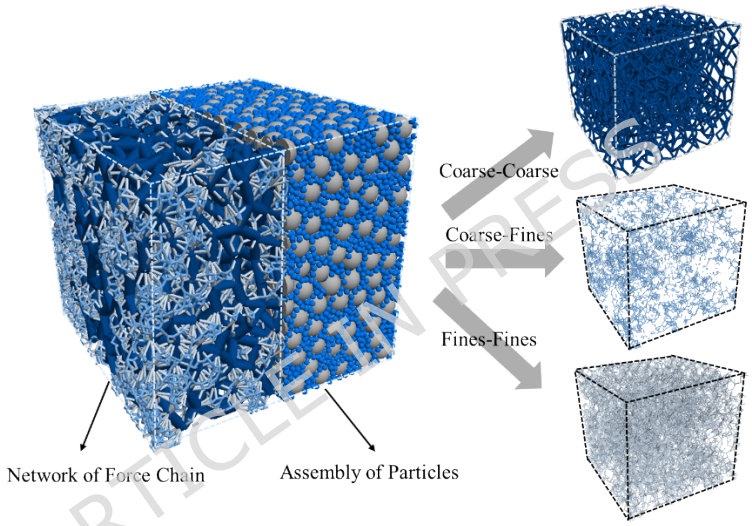

Figure 13 Sub-networks of contact force chain

The stress tensor for each of the three contact networks is calculated according to the following equation:

$$\boldsymbol{\sigma}^{k} = \frac{1}{V} \sum \boldsymbol{f}_{c}^{k} \boldsymbol{d}^{k} \tag{6}$$

Where σ^{k} represents the stress tensor of a specific contact sub-network, and the superscripts $\in$ {C-C, C-F, F-F}, denote the contact networks formed by coarse-coarse, coarse-fine, or fine-fine particles, respectively. V is the total volume of the specimen, and f_c^k and d^k are the contact force vector and branch vector, respectively, for the

contact in the sub-network. Based on the stress tensor of the contact sub-network, the shear stress and stress ratio carried by the sub-network are then calculated:

$$q^k = \sqrt{\frac{3}{2}\boldsymbol{\sigma}^{k'}\boldsymbol{\sigma}^{k'}} \tag{7}$$

$$h^k = \frac{q^k}{p} \tag{8}$$

Where $\sigma^{k'}$ is the deviatoric stress tensor of σ^k, and p is the mean effective stress of the specimen. The stress ratios of the three contact types represent the loads carried individually by the corresponding sub-networks. It should be noted that, Equation (8) uses the overall mean stress p rather than the mean stress of sub-networks p^k[61, 62], in order to allow their sum equals the overall stress ratio i.e. $h = h^{cc} + h^{cf} + h^{ff}$.

Figure 14 displays the stress ratio curves for specimens with fines contents of 5% and 20% under confining pressures of 20 kPa and 200 kPa. The contribution of C-C, C-F, and F-F contacts to the overall shear strength was calculated using the previously mentioned formulas. To highlight the effect of fines content, the stress ratio curve for the fines-free specimen (f_c = 0%) is included for comparison. For all tested specimens, regardless of the fines content or confining pressure, the F-F contacts contribute virtually no shear stress.

As shown in Figure 14(a) and (c), when the fines content is only 5%, the overall stress ratio curves are quite similar to the f_c=0% case under both high and low confining pressures. Furthermore, the stress ratio contributed by the C-F contacts is negligible.

Conversely, as shown in Figure 14(b) and (d), when the fines content is higher (f_c=20%), the overall stress ratio of the specimen increases by 0.19 and 0.24 under 20 kPa and 200 kPa confining pressures, respectively, compared to thef_c=0% case. This enhancement is because while the stress ratio carried by the C-C contacts slightly decreases, the stress ratio contributed by the C-F contacts is approximately 0.2. This significant contribution from the C-F contacts largely offsets the decrease in the C-C network and substantially increases the overall shear strength of the specimen.

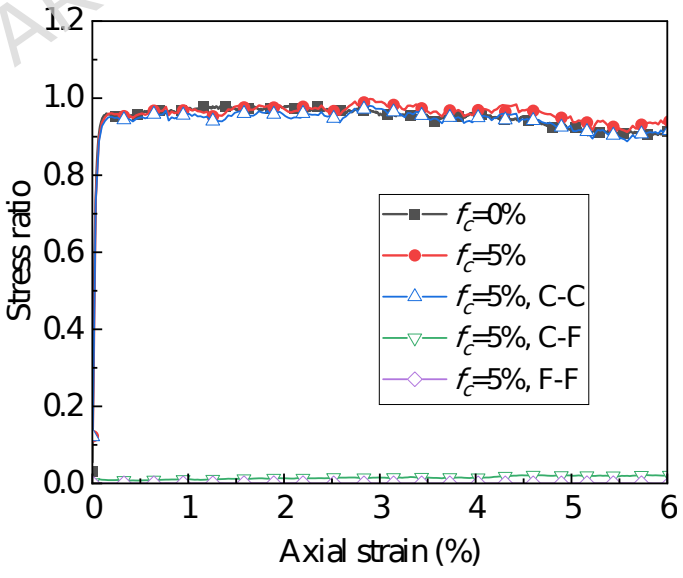

(a)

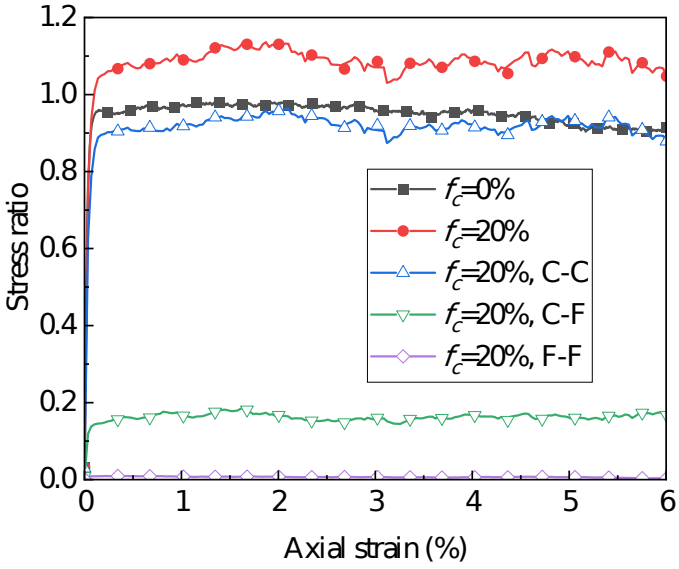

(b)

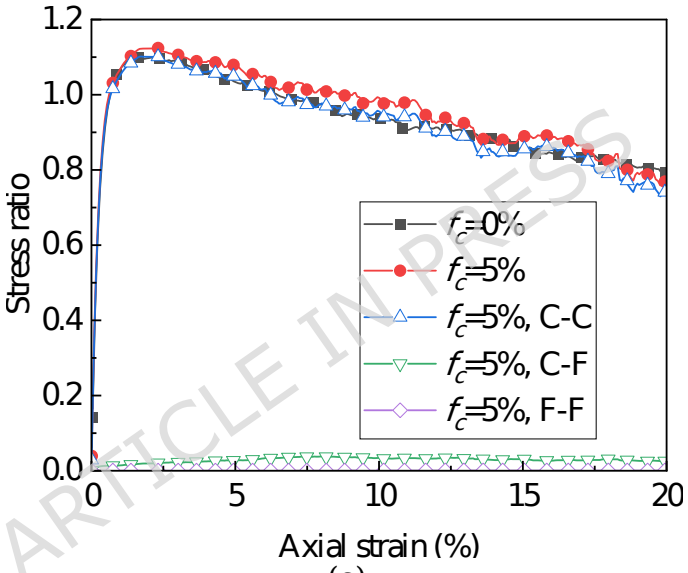

(c)

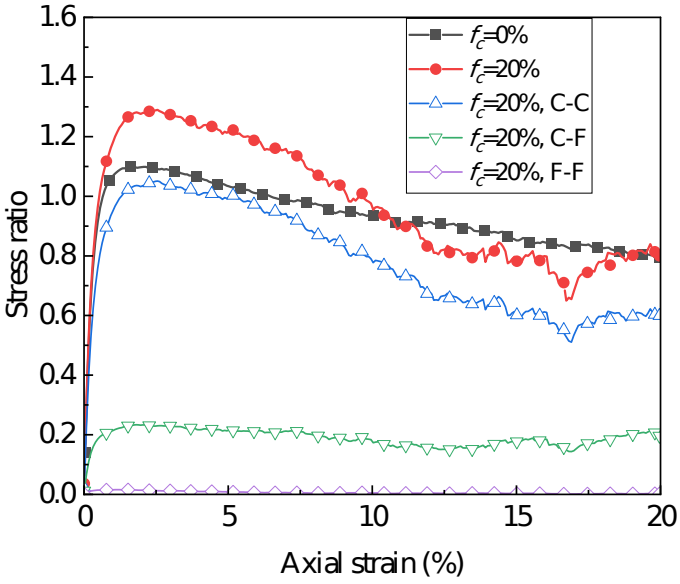

(d)

Figure 14 Stress ratio curves of specimens with different fines contents and confining pressures: (a) 20 kPa, 5%; (b) 20 kPa, 20%; (c) 200 kPa, 5%; (d) 200 kPa, 20%.

Figure 15 illustrates the variation of the stress ratio carried by the C-C and C-F contact networks with confining pressure, measured at the peak strength state for specimens with fines contents of 5% and 20%. When the fines content is only 5%, most of the load is borne by C-C contacts. However, when the fines content increases to 20%, the influence of the fine particles becomes more pronounced: (a)The load directly supported by the C-C contacts slightly decreases because some stress paths are transferred to the finer particles; (b) the newly generated C-F contacts provide additional and higher shear strength to the specimen. As the confining pressure increases from 10 kPa to 1000 kPa, the stress ratio carried by the C-F contacts increases from 0.15 to 0.29, and its proportion of the total strength contribution increases from 14.6% to 21.1%.

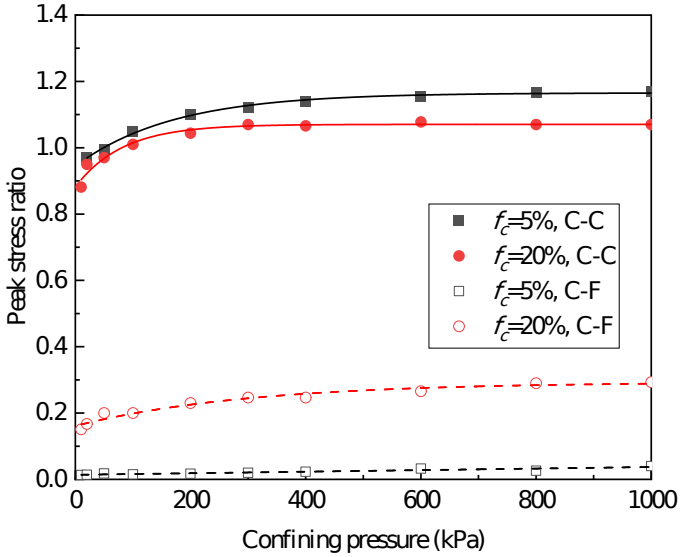

Figure 15 Decomposed stress ratios of sub-networks at the peak strength state

In summary, the variation in the trend of the peak stress ratio with confining pressure among specimens with different fines contents is due to the following reason: For specimens with high fines content (e.g., f_c=20%), although a large number of fine particles exist as rattlers at a low confining pressure of 10 kPa (approximately 80%, as shown in Figure 8), the actual load-bearing particles are sparse, resulting in low shear strength. However, with only a slight increase in confining pressure, these fine rattlers rapidly contact with coarse particles and form a more stable load-bearing network, which provides additional shear resistance to the specimen. Consequently, the peak stress ratio stabilizes within a lower confining pressure range (10~300 kPa).

New numerical cases with varying test conditions have been incorporated to verify the robustness of the findings. Specifically,

medium-dense (e_0=0.50) specimens with a fines content of 20% and a particle size ratio of 1:3 were generated using different random seeds, followed by consolidation and shearing under confining pressures of 20 and 200 kPa. The total stress ratio curves and the stress ratio curves for various contact networks are illustrated in Figure 16. It can be observed that the peak stress ratio increases with the confining pressure, which is consistent with the trend shown in Figure 12. Furthermore, the C-C contacts contribute the most to the shear strength, while the F-F contacts account for the lowest proportion, aligning with the observations in Figure 14. Consequently, the conclusions of this study are demonstrated to be highly robust.

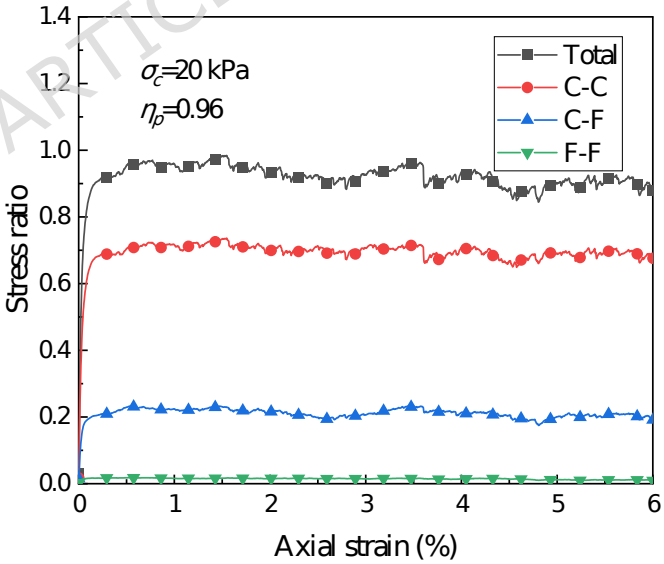

(a)

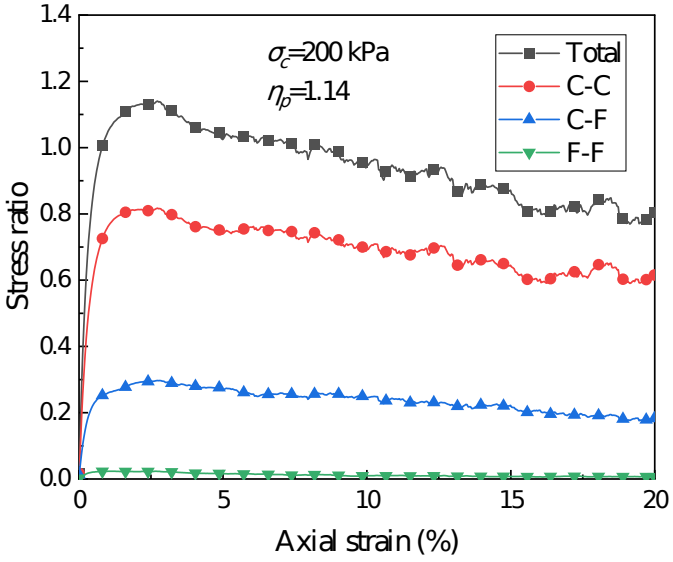

(b)

Figure 16 Stress ratio of samples with medium-dense specimens with a fines content of 20% and a particle size ratio of 1:3 generated using different random seeds: (a) σ_c=20 kPa; (b) σ_c=200 kPa

3.3 Low confining pressure failure criterion

Currently, the linear Mohr-Coulomb criterion is the most commonly used approach in engineering design to describe the strength of granular materials, assuming that the peak friction angle is only related to density and remains constant across different confining pressures [63-66]. However, addressing the nonlinear variation in the shear strength of granular materials under low confining pressures, Ling et al. [45] proposed an improved strength prediction formula:

$$h_p = A_1 \exp\left(-\frac{s_c}{p_1}\right) + h_0 \tag{9}$$

Where A_1、p_1、η_0 are fitting parameters. The peak stress ratios for different fines contents and confining pressures shown in Figure 12 were fitted using this formula, and the results are represented by

the solid lines in the figure. The fitting quality is good, with all correlation coefficients R^2 greater than 0.98. The variation of the fitted parameters p_1 and η_0 with fines content is presented in Figure 17(a) and (b), respectively, where p_1 has already been noted in Figure 12. As the fines content increases, p_1 decreases while η_0 increases. This accurately reflects the influence of fines content on the trend of the peak stress ratio shown in Figure 12: an increase in fines content leads to a higher peak stress ratio and a smaller critical confining pressure (lower critical value at low confining pressure).

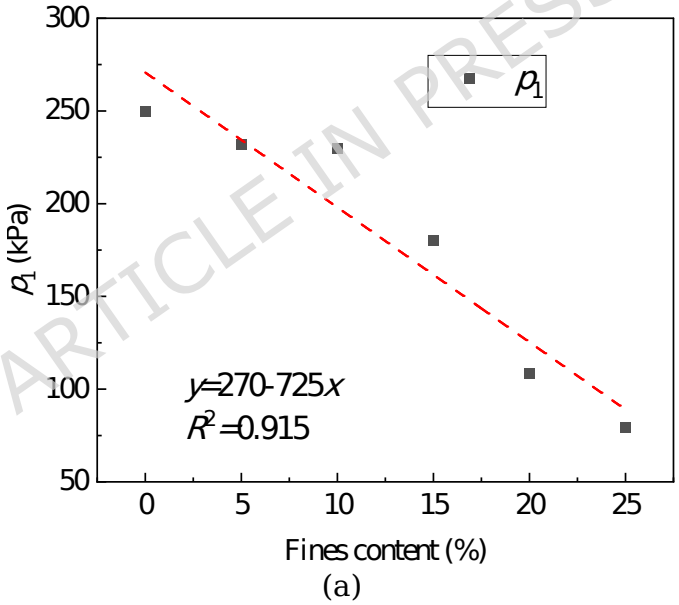

(a)

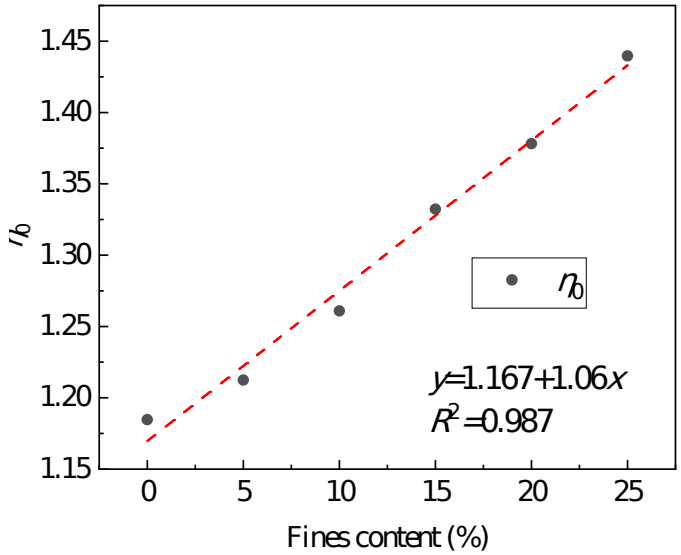

(b)

Figure 17 Variation of fitting parameters with fines content: (a)p_1; (b)η_0

Considering that the fitting parameters p_1 and η_0 exhibit an approximately linear relationship with the fines content, two linear terms with respect to f_c are introduced into Equation (8). This yields a strength criterion, presented as Equation (9), that can simultaneously reflect the influence of fines content and low confining pressures. Equation (9) expresses the peak stress ratio as a function of both confining pressure and fines content, with its mathematical expression as follows:

$$h_p(s_c, f_c) = A_1 \exp\left(-\frac{s_c}{a_f f_c + b_f}\right) + c_f f_c + h_f \tag{10}$$

Where a_f, b_f, c_f, and η_f are fitting parameters introduced to account for the effect of fines content. The parameters a_f and b_f reflect the characteristic decrease of the critical confining pressure with increasing fines content, while c_f and η_f represent the

enhancement of shear strength with increasing fines content. To capture these two aspects of the influence of fines content, Equation (9) builds upon Equation (8) by introducing only two additional fitting parameters.

The data from Figure 12 were fitted using Equation (9), and the results are presented in Figure 18. The fitted values for A_1, a_f, b_f, c_f, and η_f are -0.2740, -591 kPa, 247 kPa, 1.04, and 1.178, respectively. The correlation coefficient R^2 is 0.997. This high degree of fitting accuracy validates that the proposed equation can precisely capture the influence of fines content on the shear strength under low confining pressures.

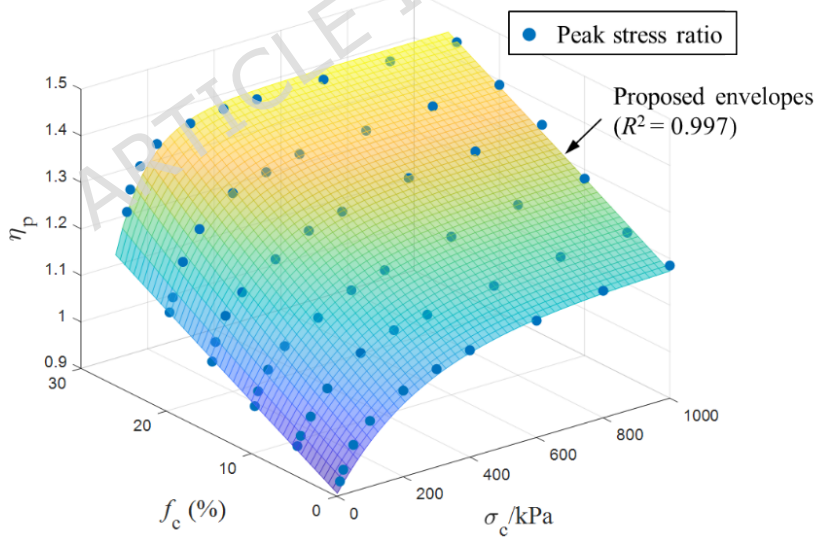

Figure 18 Strength envelope considering the influence of fines content

4 Conclusions

DEM simulations were conducted to investigate the drained triaxial behavior of spherical granular materials under varying fines contents f_c and confining pressures σ_c. The micro-mechanisms

governing the peak stress ratio were analyzed, leading to a strength prediction criterion for low-pressure conditions. Key findings are:

(1) The monotonic decrease in skeleton void ratio versus the non-monotonic trend of the global void ratio highlights a transition in the specimen's internal structure. A threshold of f_c=25% marks the transition where fine particles no longer merely occupy voids but collaboratively construct the force-chain skeleton with the coarse fraction.

(2) Under isotropic consolidation, all specimens exhibit consistent global void ratio reduction. In contrast, the evolution of skeleton void ratio is f_c-dependent: it remains relatively stable at low (f_c=5%) or high (f_c=30%) fines contents but decreases rapidly with σ_c at f_c=20%.

(3) Peak stress ratio η_p increases sharply at low σ_c before stabilizing at high σ_c. This is due to that increasing σ_c triggers a transition of rattlers into load-bearing force chains and the coarse-fine contact network provides additional shear resistance. The influence of f_c is more significant at low σ_c: higher f_c leads to a faster strength growth rate of η_p and a lower critical σ_c for stabilization. Therefore, selecting strength parameters for low-pressure engineering applications necessitates a thorough

consideration of fines content and grain size distribution

(4) A strength prediction criterion was proposed by incorporating Ω_c-dependent linear terms, effectively capturing the coupled influence of fines content and pressure. This bridges the gap between particle-scale observations and continuum-scale engineering applications.

While this study employs idealized spherical particles, it is important to consider the role of particle shape, which has a significant influence on the behaviors of granular mixtures. According to Ref. [59, 67], compared to spherical particles, irregular-shaped particles tend to decrease the fraction of rattlers while increasing the number of coarse–fine contacts, thereby enhancing the contribution of coarse–fine contacts to the overall shear strength. Future research incorporating complex particle geometries via polyhedra or clumped spheres will further refine the findings in this study.

5 Declaration of Competing Interest

The authors declare that they have no known competing financial interests or personal relationships that could have appeared to influence the work reported in this paper.

6 Availability of Data and Materials

Data will be made available on request by the corresponding

author.

7 Funding

This work was supported by China Postdoctoral Science Foundation (Grant No. 2025M773231), Department of Water Resources of Zhejiang Province, (Grant No. RA2403, RB2415), Shaanxi Province State-Owned Assets Supervision And Administration Commission (Grant No. ZXZJ-2024-049), Zhejiang Provincial Natural Science Foundation of China (Grant No. LGEZ25E090004, Grant No. LQN25D010003), Ningbo Water Resources Bureau (Grant No. NSKB202218).

8 References

1. Hongming, L., *Rail transit induced foundation settlement and Mechanistic-Empirical design method based on service performance*. 2022, Zhejiang University.
2. Zhou, C.Y., et al., *An experimental study of seabed responses around a marine pipeline under wave and current conditions.* Ocean Engineering, 2011. **38**(1): p. 226-234.
3. Wang, W., et al., *Development and management of land reclamation in China.* Ocean & Coastal Management, 2014. **102**: p. 415-425.
4. Alshibli, K.A. and A. Hasan, *Strength properties of JSC-1A lunar regolith simulant.* Journal of Geotechnical and Geoenvironmental Engineering, 2009. **135**(5): p. 673-679.
5. Xu, X.M., et al., *Correlation between liquefaction resistance and shear wave velocity of granular soils: a micromechanical perspective.* Géotechnique, 2015. **65**(5): p. 337-348.
6. Kulasingam, R., et al., *Strength loss and localization at silt interlayers in slopes of liquefied sand.* Journal of Geotechnical and Geoenvironmental Engineering, 2004. **130**(11): p. 1192-1202.
7. White, J.R.F., *A laboratory investigation into the behaviour of sand at low confining stresses*. 2020, University of Oxford: Oxford.
8. Fukushima, S. and F. Tatsuoka, *Strength and deformation characteristics of saturated sand at extremely low pressures.* Soils and Foundations, 1984. **24**(4): p. 30-48.
9. Tatsuoka, F., S. Goto, and M. Sakamoto, *Effects of some factors on strength and deformation characteristics of sand at low pressures.* Soils and Foundations, 1986. **26**(1): p. 105-114.
10. Lehane, B.M. and Q.B. Liu, *Measurement of shearing characteristics of granular materials at low stress levels in a shear box.* Geotechnical and Geological Engineering, 2012. **31**(1): p. 329-336.

11. Gu, X.Q., J.C. Zhang, and X. Huang, *DEM analysis of monotonic and cyclic behaviors of sand based on critical state soil mechanics framework.* Computers and Geotechnics, 2020. **128**: p. 103787.
12. Zhao, J.D. and N. Guo, *The interplay between anisotropy and strain localisation in granular soils: a multiscale insight.* Géotechnique, 2015. **65**(8): p. 642-656.
13. Ponce, V.M. and J.M. Bell, *Shear strength of sand at extremely low pressures.* Journal of Soil Mechanics & Foundations Div, 1971.
14. Indraratna, B., D. Ionescu, and H. Christie, *Shear behavior of railway ballast based on large-scale triaxial tests.* Journal of geotechnical and geoenvironmental Engineering, 1998. **124**(5): p. 439-449.
15. Hasan, A. and K.A. Alshibli, *Discrete element modeling of strength properties of Johnson Space Center (JSC-1A) lunar regolith simulant.* Journal of Aerospace Engineering, 2010. **23**(3): p. 157-165.
16. Nguyen, H.B.K., M.M. Rahman, and A.B. Fourie, *Characteristic behavior of drained and undrained triaxial compression tests: DEM study.* Journal of Geotechnical and Geoenvironmental Engineering, 2018. **144**(9): p. 04018060.
17. Yang, X., et al., *Effect of particle morphology on strength of glass sands.* International Journal of Geomechanics, 2023. **23**(8): p. 04023117.
18. Sitharam, T.G. and J.S. Vinod, *Critical state behaviour of granular materials from isotropic and rebounded paths: DEM simulations.* Granular Matter, 2009. **11**(1): p. 33-42.
19. Vinod, J.S., B.V. Ravishankar, and T.G. Sitharam, *Evaluation of undrained response from drained triaxial shear tests: DEM simulations and experiments.* Géotechnique, 2008. **58**(7): p. 605-608.
20. Jiang, H., et al., *Numerical identification of size-shape-strength attractors in sheared breakable granular materials.* Computers and Geotechnics, 2026. **190**.
21. Ishihara, K., *Liquefaction and flow failure during earthquakes.* Geotechnique, 1993. **43**(3): p. 351-451.
22. Wang, X.K., et al., *Microscopic mechanism and analytical modeling of seepage-induced erosion in bimodal soils.* Computers and Geotechnics, 2022. **141**: p. 104527.
23. O'Sullivan, C., K. Hanley, and R. Fannin, *Fabric and effective stress distribution in internally unstable soils.* Journal of geotechnical and geoenvironmental engineering, 2014. **140**(12): p. 04014072.
24. Thevanayagam, S. and G.R. Martin, *Liquefaction in silty soils—screening and remediation issues.* Soil Dynamics and Earthquake Engineering, 2002. **22**(9–12): p. 1035-1042.
25. Seed, H.B., *Design problems in soil liquefaction.* Journal of Geotechnical Engineering, 1987. **113**(8): p. 827-845.
26. Pitman, T., P. Robertson, and D. Sego, *Influence of fines on the collapse of loose sands.* Canadian Geotechnical Journal, 1994. **31**(5): p. 728-739.
27. Ni, Q., et al., *Contribution of fines to the compressive strength of mixed soils.* Géotechnique, 2004. **54**(9): p. 561-569.
28. Lade, P.V. and J.A. Yamamuro, *Effects of nonplastic fines on static liquefaction of sands.* Canadian Geotechnical Journal, 1997. **34**(6): p. 918-928.
29. Monkul, M.M. and J.A. Yamamuro, *Influence of silt size and content on liquefaction behavior of sands.* Canadian Geotechnical Journal, 2011. **48**(6): p. 931-942.
30. Yang, J. and L.M. Wei, *Collapse of loose sand with the addition of fines: the role of particle shape.* Géotechnique, 2012. **62**(12): p. 1111-1125.
31. Chung, Y.-C., C.-C. Liao, and Z.-H. Zhuang, *Experimental investigations for the effect of fine powders on size-induced segregation in binary granular mixtures.* Powder Technology, 2021. **387**: p. 270-276.
32. Liao, C.-C., et al., *Influences of fine powder on dynamic properties and density segregation in a rotating drum.* Advanced Powder Technology, 2020. **31**(4): p. 1702-1707.

33. Gong, J., et al., *Exploring the effects of particle shape and content of fines on the shear behavior of sand-fines mixtures via the DEM.* Computers and Geotechnics, 2019. **106**: p. 161-176.
34. Hu, T., et al., *Evolution of rattlers under different confining pressures and its influence on shear strength.* Transportation Geotechnics, 2024. **44**: p. 101176.
35. Dai, B.B., J. Yang, and X.D. Luo, *A numerical analysis of the shear behavior of granular soil with fines.* Particuology, 2015. **21**: p. 160-172.
36. Itasca Consulting Group Inc., *PFC3D – Particle Flow Code in 3 Dimensions, Ver. 5.0*. 2015: Minneapolis.
37. Zhao, S., T.M. Evans, and X. Zhou, *Effects of curvature-related DEM contact model on the macro- and micro-mechanical behaviours of granular soils.* Géotechnique, 2018. **68**(12): p. 1085-1098.
38. Liu, D., et al., *The role of particle shape in stress transmission and stiffness in gap-graded soils.* Computers and Geotechnics, 2026. **192**.
39. Zuo, L. and B.A. Baudet, *Determination of the transitional fines content of sand-non plastic fines mixtures.* Soils and Foundations, 2015. **55**(1): p. 213-219.
40. Liang, W., et al., *Scalable three - dimensional hybrid continuum - discrete multiscale modeling of granular media.* International Journal for Numerical Methods in Engineering, 2022. **123**(12): p. 2872-2893.
41. Wu, K., et al., *Study of shear behavior of granular materials by 3D DEM simulation of the triaxial test in the membrane boundary condition.* Advanced Powder Technology, 2021. **32**(4): p. 1145-1156.
42. Lee, S.J., Y.M. Hashash, and E.G. Nezami, *Simulation of triaxial compression tests with polyhedral discrete elements.* Computers and Geotechnics, 2012. **43**: p. 92-100.
43. Terzaghi, K., R.B. Peck, and G. Mesri, *Soil mechanics in engineering practice*. 1996: John wiley & sons.
44. Goldenberg, C. and I. Goldhirsch, *Friction enhances elasticity in granular solids.* Nature, 2005. **435**(7039): p. 188-191.
45. Ling, D., et al., *Numerical study on the shear strength of granular materials under the low confining pressure.* Soils and Foundations, 2024. **64**(3): p. 101447.
46. Christoffersen, J., M.M. Mehrabadi, and S. Nemat-Nasser, *A Micromechanical Description of Granular Material Behavior.* Journal of Applied Mechanics, 1981. **48**(2): p. 339.
47. Li, X., H.S. Yu, and X.S. Li, *A virtual experiment technique on the elementary behaviour of granular materials with discrete element method.* International Journal for Numerical and Analytical Methods in Geomechanics, 2011. **37**(1): p. 75-96.
48. Wu, Q.X., K. Pan, and Z.X. Yang, *Undrained cyclic behavior of granular materials considering initial static shear effect: Insights from discrete element modeling.* Soil Dynamics and Earthquake Engineering, 2021. **143**.
49. Gu, X., M. Huang, and J. Qian, *DEM investigation on the evolution of microstructure in granular soils under shearing.* Granular Matter, 2013. **16**(1): p. 91-106.
50. Zuo, K.L., et al., *Exploring packing density, critical state, and liquefaction resistance of sand-fines mixture using DEM.* Computers and Geotechnics, 2023. **156**: p. 105278.
51. Zhou, W., et al., *Effects of particle size ratio on the macro-and microscopic behaviors of binary mixtures at the maximum packing efficiency state.* Granular Matter, 2016. **18**(4): p. 81.
52. Da Cruz, F., et al., *Rheophysics of dense granular materials: Discrete simulation of plane shear flows.* Physical Review E—Statistical, Nonlinear, and Soft Matter Physics, 2005. **72**(2): p. 021309.
53. Lopera Perez, J.C., et al., *Assessing the quasi-static conditions for shearing in granular media within the critical state soil mechanics framework.* Soils and Foundations, 2016. **56**(1): p. 152-159.

54. Huang, X., et al., *Exploring the influence of interparticle friction on critical state behaviour using DEM.* International Journal for Numerical Analytical Methods in Geomechanics, 2014. **38**(12): p. 1276-1297.
55. Yang, J., L.M. Wei, and B.B. Dai, *State variables for silty sands: Global void ratio or skeleton void ratio?* Soils and Foundations, 2015. **55**(1): p. 99-111.
56. Kumar, N., et al., *Tuning the bulk properties of bidisperse granular mixtures by small amount of fines.* Powder Technology, 2016. **293**: p. 94-112.
57. Ng, T.-T., et al., *Macroscopic and microscopic behaviors of binary mixtures of different particle shapes and particle sizes.* International Journal of Solids and Structures, 2018. **135**: p. 74-84.
58. Cantor, D. and C. Ovalle, *Sample size effects on the critical state shear strength of granular materials with varied gradation and the role of column-like local structures.* Géotechnique, 2025. **75**(1): p. 29-40.
59. Hu, T.-T., et al., *Numerical study on the shear strength under low confining pressure of sandy soils with different particle shapes.* Transportation Geotechnics, 2025. **55**.
60. Gong, J., et al., *Exploring the effects of particle shape and content of fines on the shear behavior of sand-fines mixtures via the DEM.* Computers and Geotechnics, 2019. **106**: p. 161-176.
61. Papadopoulos, L., et al., *Network analysis of particles and grains.* Journal of Complex Networks, 2018. **6**(4): p. 485-565.
62. Kawamoto, R., J. Andrade, and T. Matsushima, *A 3-D mechanics-based particle shape index for granular materials.* Mechanics Research Communications, 2018. **92**: p. 67-73.
63. Bishop, A.W., *The strength of soils as engineering materials.* Géotechnique, 1966. **16**(2): p. 91-130.
64. Acar, Y.B., H.T. Durgunoglu, and M.T. Tumay, *Interface properties of sands.* Journal of the Geotechnical Engineering Division, 1982. **108**(4): p. 648-654.
65. Cornforth, D.H., *Some experiments on the influence of strain conditions on the strength of sand.* Géotechnique, 1964. **14**(2): p. 143-167.
66. Schmertmann, J.H., *Guidelines for cone penetration test: performance and design*. 1978, United States. Federal Highway Administration.
67. Liu, X., et al., *Synergistic effects of particle shape and size distributions on the maximum shear modulus of granular materials: A DEM-based investigation.* Construction and Building Materials, 2026. **506**.

9 Author contributions statement

Tiantian Hu: Original draft, Project administration, Formal analysis. Gao Zhicheng: Review & editing, Software. Zhang Chaojie: Funding acquisition, Investigation. Jing Wang: Resources, Data curation.